

STELLAR OSCILLATIONS TIDALLY INDUCED BY A PLANETARY COMPANION

ANDREW BUNTING

ABSTRACT. A stellar oscillation code using the Henyey method to solve for the non-radial oscillations induced as a result of a companion planet's tidal potential is built and tested.

After some general testing to ensure the numerical aspect of the code produces accurate solutions, the case of a Hot Jupiter orbiting a solar-type star is tested, and is found to agree well with previously published results. The limitations of the code are explored, including the effects of varying the semi-major axis of the planetary orbit, and of varying the resolution.

The future prospects for this project, including the application to particular physical systems, the production of predicted results of observations, and the application to non-solar-type stars such as Red Giants and White Dwarfs, are discussed. There is scope for extending the code, broadening its range of applicability to include eccentric orbits, rotating stars and higher order modes of oscillation.

1. INTRODUCTION

Stars are ubiquitous in almost all areas of astrophysics, and it is becoming increasingly apparent that planets are a common occurrence as well. My project revolves around the interaction between a subset of these two very common objects, and will enable the effect of tidally-driven stellar oscillations to be modelled, in order to assess their effect on the detection of planets.

Over the course of the introduction I will set out the background to the project, including setting it in a (brief) history of the relevant areas, covering: Asteroseismology, Stellar Oscillations, Stellar Structure, Exoplanets and Tidal Asteroseismology. In the sections following that, I will cover in some more detail the Henyey method, the implementation of the method for this particular set of equations, and the outputs generated by the code; I will end with a conclusion of what has been achieved, and a plan for future work to further these achievements.

1.1. Hot Jupiters. In 1989 the first exoplanet was unknowingly detected by Latham *et al* [14], thought at the time to be a brown dwarf, and later acknowledged as a gas giant with a minimum mass of $11 M_{Jup}$ [22]. This was followed by the first exoplanet discovery in 1995 [16]: 51 Pegasi b, another gas giant orbiting a solar-type star. Since then, many more exoplanets have been discovered [17], a large number of them being gas giants in close orbits [23].

The reason that selection effects favour the detection of Hot Jupiters (that is, planets of about a Jupiter mass, with semi-major axes up to approximately 0.1 au) is due to their two primary characteristics: they are massive, and close to their star. These effects

combine to have the greatest gravitational influence on the star, giving a large radial velocity (RV) signal, as well as a wider range of angles from which a transit can be observed, and the short period of the orbits enables periodicity to be well established over a shorter time than for planets with larger semi-major axes. Given that most early detections came through RV measurements, and the huge success of Kepler and K2 using the transit method [4], the current population of detected exoplanets should not be understood to be a representative sample, but its preferential selection is useful for the purposes of this project.

1.2. Asteroseismology. Variable stars have been observed for over 3000 years [12], although only in the last few centuries has the number of observed variable stars really grown [11]. That stars are not constant was a major change from the classical view of the celestial sphere, and adds many layers to the complexity of stars, but also introduces new ways for us to learn about them. Asteroseismology is the study of stellar oscillations, and is a rapidly growing field, as the quality of observations of stellar surfaces continues to improve.

Asteroseismology, understandably, first came about in studying the oscillations of our very own star – potentially the first such vibrations were observed by Plaskett in 1916 [20], although at the time the observed variation in solar rotation was thought to be due to some atmospheric effects, this was shown not to be the case by Hart in 1954 [9]. Since then, thousands of solar oscillation modes have been observed, each one enabling a subtly different probe of the solar interior [7]. The most prominent mode has a period of around 5 minutes, and decays rapidly (over a few periods) [21], and is thought to be driven by convective motions inside the sun, although this is still an area of active research. Observations of oscillations on other stars soon followed [1], including the detection of individual modes of oscillation on η Bootis in 1995, although this was also unclear until it was confirmed in 2003 [13].

The study of these modes of oscillation is a generalised version of the study of variable stars such as δ Scuti stars, the brightest of which oscillate in a spherically symmetric manner as opposed to the not purely radial oscillations which are harder to observe [8]. They have a clearly dominant mode of pulsation, with large variation in their physical properties (the variation in magnitude can exceed 0.5 mag [8]). An obvious wider application of the study of stellar oscillations is the use of Cepheid variables to determine a cosmic distance scale [15].

The great benefit in studying these oscillations is the fact that they are oscillations throughout the body star, not merely at the surface. This allows the interior structure of the star to be assessed much more readily than observations which depend only on the surface properties of the star. This has been applied in several ways, such as using asteroseismology to determine properties of stars, including precise estimates of their ages [3] [6].

The relevance of stellar oscillations to this project is the effect that these oscillations have on the detection of planets. A moving stellar surface will introduce a doppler shift which varies periodically, just as the gravitational effect of the Hot Jupiter causes the periodic RV variation which enables the planet to be detected. The flux will also be perturbed, which will cause a periodic change in the brightness of the star, which has implications for the use of photometric measurements in detecting transiting planets.

The precise nature and magnitude of these effects, and the implications for detecting further planets around such stars, is the subject of this project. A multiplanet system would have an RV signal which is a superposition of the influence of all the planets, and would therefore include multiple different frequencies in the power spectrum, it is important to understand precisely what modes will be excited by the first planet, in order to clearly remove the total effect from the first planet before any subsequent detections can be assessed. This has a twofold effect, first in preventing any false positives from higher frequency oscillations from the Hot Jupiter being designated as being due to other planets, and also reducing the background noise in the power spectrum, so that any signal not due to the Hot Jupiter could be more clearly seen.

As a secondary benefit, as it is another way to observe the system, it could be used to better constrain properties of the system. For instance, the properties of the system, such as the semi-major axis of the planet's orbit, or the inclination of the orbit could be constrained by comparing the measured amplitude of oscillations to the modelled values. Or, if the orbital system is already well constrained, tidal asteroseismology could be used to test the accuracy of the stellar model, and could diagnose where failings in the modelling are particularly problematic by contrasting the modelled stellar structures where the observations and theory don't match to those where they do match. There is a range of stars with Hot Jupiters which have been observed by radial velocity measurements, including some which have multiple planets [17]. As objects of interest from Kepler are followed up, however, this breadth of radial velocity measurements will increase this range [5].

1.3. Computing Stellar Oscillations. In order to quantitatively study these oscillations, a system of equations to describe them must be used. In order to be able to derive this set of equations, the following assumptions must be made.

Time independence: The equilibrium structure of the star changes on a time-scale much longer than that of the oscillations.

Spherical symmetry: The equilibrium structure of the star is totally spherically symmetric, parametrised as a function only of the radius. This enables the effective use of spherical harmonics to simplify things throughout the derivation.

Static state: Fluid velocity of the equilibrium state is negligible compared to the motions of the oscillations.

Cowling approximation: The perturbation to the self-gravity potential due to the deformation of the star in the process of oscillating is negligible compared to the perturbation which incites the oscillations.

Small perturbation: The perturbation must be small, so that the linearised regime is a valid approximation.

Wave solutions: We use wavelike solutions, with a time dependence of $e^{im\omega t}$, where m is the order of the spherical harmonic and ω is the angular frequency of the planet's orbit.

To start with, 12 hydrodynamic and thermodynamic equations are linearised and expressed in terms of spherical harmonics. The undesirable perturbed variables are eliminated, to leave four first order linear differential equations in terms of ξ_r , F'_r , p' and T' ; the radial displacement, perturbation to the radial flux, perturbation to the pressure

and perturbation to the temperature. A more complete derivation is given in appendix A.

The final form of the equations which are to be solved is as follows:

$$(1) \quad \frac{1}{\rho_0 R} \frac{\partial}{\partial r} \left(\rho_0 r^2 \tilde{\xi}_r \right) + \left(\frac{r^2}{\chi_\rho R^2} - \frac{l(l+1)p_0}{m^2 \omega^2 R^2 \rho_0} \right) \tilde{p} - \frac{\chi_T}{\chi_\rho} \frac{r^2}{R^2} \tilde{T} = \frac{l(l+1)r^2 f}{m^2 \omega^2 R^2}$$

$$(2) \quad iA \frac{\chi_\rho}{\chi_T} \frac{r}{R} \tilde{\xi}_r + \frac{F_{r_{BC}}}{m\omega\rho_0 T_0 c_p R^2} \frac{\partial}{\partial r} \left(r^2 \tilde{F}_r \right) - i\nabla_{ad} \frac{r^2}{R^2} \tilde{p} + \left(i \frac{r^2}{R^2} + \frac{l(l+1)K_0}{\rho_0 m \omega c_p R^2} \right) \tilde{T} = 0$$

$$(3) \quad - \frac{F_{r_{BC}}}{K_0} \frac{\partial r}{\partial T_0} \tilde{F}_r + \frac{1}{\chi_\rho} \left(1 + \frac{1}{\kappa_0} \left(\frac{\partial \kappa_0}{\partial \ln \rho_0} \right)_{T_0} \right) \tilde{p} + \left(-4 + \frac{1}{\kappa_0} \left(\frac{\partial \kappa_0}{\partial \ln T_0} \right)_{\rho_0} - \frac{\chi_T}{\chi_\rho} \left(1 + \frac{1}{\kappa_0} \left(\frac{\partial \kappa_0}{\partial \ln \rho_0} \right)_{T_0} \right) \right) \tilde{T} - T_0 \frac{\partial \tilde{T}}{\partial T_0} = 0$$

$$(4) \quad -\tilde{\xi}_r + \frac{1}{m^2 \omega^2 R} \left(\frac{1}{\rho_0} \frac{\partial (p_0 \tilde{p})}{\partial r} + \frac{g_0}{\chi_\rho} \tilde{p} \right) - \frac{\chi_T g_0}{\chi_\rho m^2 \omega^2 R} \tilde{T} = -\frac{2f}{m^2 \omega^2} \frac{r}{R}$$

where the variables being solved for are:

$$(5) \quad \tilde{\xi}_r \equiv \frac{\xi_r}{R}$$

$$(6) \quad \tilde{F}_r \equiv \frac{F'_r}{F'_{r_{BC}}}$$

$$(7) \quad \tilde{p} \equiv \frac{p'}{p_0}$$

$$(8) \quad \tilde{T} \equiv \frac{T'}{T_0}$$

The subscript 0 refers to the equilibrium state, and primes refer to the perturbation to that equilibrium. The variables that have not yet been defined are: ρ , the density; R , the radius at the surface of the star; r the radius at that point in the star; p , pressure; T , temperature; F_r , the radiative flux; $F_{r_{BC}} = F_{r_0}|_{r=R}$; l , the degree of the spherical harmonic being solved for; m , the order of the spherical harmonic; ω , the angular frequency of the planet's orbit; f , a measure of the tidal perturbation, an overview of which is in the following section; c_p , the specific heat capacity at constant pressure; K , the radiative thermal conductivity; $\chi_\rho \equiv \left(\frac{\partial \ln p}{\partial \ln \rho} \right)_T$; $\chi_T \equiv \left(\frac{\partial \ln p}{\partial \ln T} \right)_\rho$; κ , the opacity; g , the magnitude of the gravitational acceleration; $A = \frac{N^2}{g_0} r$, as it is defined in MESA, using

the Brunt-Väisälä frequency, N ; and $\nabla_{ad} = \left(\frac{\partial \ln T_0}{\partial \ln p_0} \right)_{s_0} = \frac{p_0}{T_0} \left(\frac{\partial T_0}{\partial p_0} \right)_{s_0}$, where s is the specific entropy.

The equations 1 to 4 solve for the non-adiabatic case of a perturbation expressed as a single spherical harmonic. Any perturbation can be expressed as a sum of spherical harmonics, and the equations are linear, so the solutions can be summed. This enables any perturbation to be broken down into its component spherical harmonics, and solved for each value of l and m . The full solution is then the sum of these individual solutions. The particular form of the equations has implications for the numerical solution, and this form has been chosen as it is dimensionless, and is solved accurately in the test cases.

In this project, the perturbation is caused by the tidal potential of the companion planet, which takes the form of the non-zero terms on the right hand sides of equations 1 and 4. This arises from consideration of the lowest order, time-dependent, spatially varying term of the perturbing body's potential. We work in the (non-inertial) frame centred on the star. As such, we need not consider the first order effect of the planetary companion, which causes the motion of the star about the system's common centre of mass.

This leads to the tidal potential as:

$$(9) \quad \phi_T \approx -\frac{Gm_p}{4D} \left(\frac{r}{D} \right)^2 P_2^2(\cos(\theta)) e^{2i(\omega t - \phi)}$$

where ϕ_T is the tidal potential; G is the gravitational constant; m_p the mass of the planet; D the distance between the centre of the star and the centre of the planet; t , time; ϕ , the azimuthal angle; θ , the polar angle; $P_2^2(\cos(\theta))$ is the associated Legendre polynomial with $l = 2$ and $m = 2$, equal to $3\sin^2(\theta)$.

The non-radial dependence and time dependence can be cancelled out, as all the variables have it in common, leaving only the radial dependence of the perturbation:

$$(10) \quad \Phi_P = -\frac{Gm_p}{4D} \left(\frac{r}{D} \right)^2 = -\frac{Gm_p}{4D^3} r^2 = fr^2$$

where Φ_P is the radial tidal potential, and $f = -\frac{Gm_p}{4D^3}$.

2. THE HENYEY METHOD

This method for solving equations was set out by Henyey *et al* in 1964 [10], as a method for computing stellar evolution, and will be explained throughout this section.

2.1. A general introduction to the method. To start with, the structure of the equations must be set out. This method is used to solve four linear, first order differential equations. Whilst it is not necessary in general, here we will be restricting ourselves to the case where the two pairs of variables are on a staggered grid, with \vec{u} being evaluated at the outer edge of the cell, and \vec{v} being evaluated at the centre of the cell, where $\vec{u} = (a, b)^T$ and $\vec{v} = (c, d)^T$

The boundary equations are split, two apply at the centre ($\vec{u} = 0$) and two apply at the surface of the star. Because of this, it is difficult to work with a solution from one boundary to the other, as the problem is under-constrained until all boundary conditions can be applied. It is this splitting of the boundary conditions, combined with the potentially highly oscillatory nature of the solutions, which means that other methods, such as the Shooting Method, would be difficult to reliably implement, and therefore we have opted for the Henyey method.

In order to get around this, the Henyey method uses a two-stage approach. A relation between \vec{u} and \vec{v} is used, which is formulated in such a way that conditions upon the coefficients can be found which reproduce the central boundary condition. This relation is

$$(11) \quad \vec{u}_k + \underline{\alpha}_k \vec{v}_k + \vec{\gamma}_k = 0,$$

which obeys the central boundary condition if $\underline{\alpha}_0 = 0$ and $\vec{\gamma}_0 = 0$ are used as a surrogate. Recurrence relations for the coefficients in this equation ($\underline{\alpha}$ and $\vec{\gamma}$) are used to calculate the values of these coefficients at each point, including at the surface. Using the surface boundary conditions with the outermost coefficients, the values for \vec{u} and \vec{v} can be evaluated. Then, another recurrence relation can be found, which relates the values of $\underline{\alpha}$, $\vec{\gamma}$, \vec{u} and \vec{v} at a given point, to the values of \vec{u} and \vec{v} at the adjacent point just inside. This enables them to be evaluated at all points throughout the star, and the solution is complete. This is the essential idea of this method, and has been set out diagrammatically in figure 1.

To describe this problem more specifically, we must look at the structure of the equations in question (see appendix A), and the variables involved. Two equations involve the derivative of \vec{u} but not \vec{v} , and the other two include the derivative of \vec{v} but not \vec{u} . Because of this, we can split the four equations into two matrix equations:

$$(12) \quad \underline{A}_{k,k+1} \vec{u}_k + \underline{C}_{k,k+1} \vec{u}_{k+1} + \underline{D}_{k,k+1} \vec{v}_{k+1} = \vec{M}_{k,k+1},$$

$$(13) \quad \underline{E}_{k,k+1} \vec{u}_k + \underline{F}_{k,k+1} \vec{v}_k + \underline{H}_{k,k+1} \vec{v}_{k+1} = \vec{N}_{k,k+1}.$$

This structure means that the two equations with derivatives of \vec{u} make up equation 12, which is evaluated at the midpoint of cell $k+1$; and the two equations with derivatives of \vec{v} make up equation 13, which is evaluated at the outer edge of cell k . Notably, this structure ensures that the matrices B and G , which would be included in a more general formulation, are ignored from the start, as they would be null at all points, which helps to avoid issues like trying to invert a singular matrix. In this discussion, the star is divided into J cells, so k will run from 0 to $J - 2$ (as the $k = J - 1$ would require $k + 1 = J$, which would be outside the star).

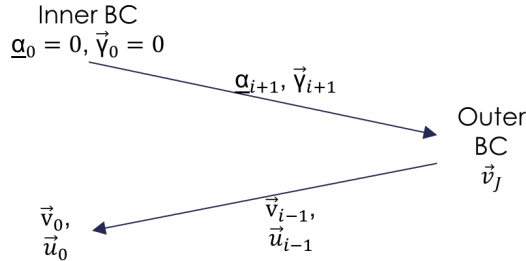


FIGURE 1. A diagrammatic overview of the Henyey method, showing what is being evaluated at each stage of the code. The arrows represent the two recurrence relations, with the inwards arrow progressively calculating the solution as it works back towards the centre of the grid.

This code was built from scratch, and tested extensively in various situations, particularly assessing the differences between analytically equivalent expressions of the recurrence relations and the differences between different applications of the boundary conditions. The numerical components were also extensively tested, including ensuring the accuracy of matrix and vector manipulation, particularly matrix inversion in the case of small determinants; a structure to deal with the manipulation of complex numbers was included and tested; and a method of interpolation of input data was built, such that the maximum cell size could be precisely controlled and varied across the grid. These were used to solve a variety of different equations, ranging from simple algebraic equations up to the complex differential equations which are used to solve the stellar oscillation equations.

3. IMPLEMENTING THE EQUATIONS

This section discusses the more specific implementation of the stellar oscillation equations, including the problems associated with that, and how they were addressed and overcome.

3.1. Choosing the form of the equations. Once a general Henyey code has been successfully built and tested, the first stage in applying it to a specific problem is to change the equations which it is solving. However, this is not a simple task, as the form of the equations and the precise form of the variables which are being solved for affects the accuracy of the code. The primary thing to avoid is for any variable, term, or matrix component to be divided by anything which goes to 0. It is important to be mindful of the fact that the term is split over the course of the solution, and that checking that the equation itself has no poles is insufficient.

As such, in making the equations and variables dimensionless, I avoided dividing anything by r , g_0 , F_{r_0} , or any other variable which goes to 0 at any point. This resulted in the normalisations of variables as:

$$(14) \quad \tilde{\xi}_r \equiv \frac{\xi_r}{R}$$

$$(15) \quad \tilde{F}_r \equiv \frac{F_r}{F_{r_{BC}}}$$

$$(16) \quad \tilde{p} \equiv \frac{p}{p_0}$$

$$(17) \quad \tilde{T} \equiv \frac{T}{T_0}$$

where $F_{r_{BC}} = F_{r_0}|_{r=R}$. This, combined with the careful treatment of the oscillation equations, was found to converge well to the solution when used with dummy test cases where the answers are fully known analytically.

3.2. Discretisation. The code does not directly take the equations as an input, but rather takes the form of the matrices A to H , the vectors M and N (as well as the corresponding matrices and vectors in the outer boundary condition). Therefore the equations must be expressed in a discretised form, but efforts must be made to minimise the loss of accuracy as a result of this.

The primary way of achieving this is to be very careful about where variables are defined, and where the equations are being evaluated. To determine where each equation is being evaluated, one must consider which derivatives are present in the equation, and one must only use variables from cells k and $k + 1$. For equation 12 this is the centre of cell $k + 1$, and is therefore fairly simple: the cell-centre variables are simply given by their $k + 1$ value, the cell-face variables are given by a simple average of the k and $k + 1$ values. For equation 13, however, things are not so simple, as this equation must be evaluated at the face of cell k , and adjacent cells need not be the same size. Although most adjacent cells will be of a similar size, on some occasions, such as towards the very centre or outer edge of the star, the cell size may vary rapidly in size. In this case, the cell-face variables are simply given by their k value, but the cell-centre variables must be evaluated using a weighted average, essentially linearly interpolating between the two known values to estimate the value at the face of cell k . It must be noted, however, that this scheme of averaging is only effective if the variables can be approximated well by a linear variation over the range of the two cells, which necessitates a sufficiently fine grid.

The derivatives as a whole must also be treated carefully. In an attempt to prevent introducing extra sources of numerical inaccuracy, derivatives of multiple variables are, where possible, expressed as a single derivative, rather than expanding the term using the chain rule. Whilst this may have some drawbacks in cases of different size cells where the derivative is non-linear (although this would again be minimised by increasing the resolution), it is more stable against potential poles in any individual variable involved in the derivative.

3.3. Input data. As the equations work by perturbing an equilibrium model of the star, the code requires that this equilibrium state be provided as an input. As mentioned in section ??, this stellar model is created using MESA. Once created, data about the properties of the star can be extracted and formatted to be used as an input for the

Henyey code, and with this the variables are already split into cell-centre and cell-face types, and the data is output on a discrete grid. This defines the underlying grid for the implementation of the Henyey code, but is insufficient for our purposes.

In order to use this data in a satisfactory manner, the grid must be made sufficiently fine across the whole star, with particularly fine resolution in areas which give a highly spatially oscillatory response (that is expected to be the radiative regions, where solutions are expected to be oscillatory, whereas they are expected to be evanescent in convective zones). This requires that new points be added to the grid, requiring both interpolating the input data, and controlling the maximum cell size throughout the star.

These two processes are obviously intimately related, as neither can effectively occur without the other. The resolution is controlled by setting a maximum cell size as a function of position in the star, and splitting any cells which exceed that size. The difficulty comes about when trying to split the cells whilst still keeping track of how the old arrays containing the input data correspond to the new, higher resolution, arrays which must be filled with accurately interpolated data. Controlling the accuracy of the interpolation requires control of the process of generating the grid within MESA, by setting maximum changes in variables between adjacent cells to a suitable value such that the linear interpolation scheme is valid. A particular problem with this is the fact that the parts of the star that MESA requires highest resolution for are not necessarily the parts which the Henyey code requires highest resolution for, particularly for central radiative zones, which MESA regards as simple to model, but in which the very highest (spatial) frequency oscillations occur. Another potential problem is the fact that cell-centre variables, in order to be strictly interpolated rather than extrapolated, are not simply a weighted average of their $k - 1$ and k values, but, for adding cells to the outer half of a cell, require interpolating between k and $k + 1$. This asymmetry in the interpolation of cell-centre variables compared to cell-face variables could potentially lead to artificially large derivatives evaluated in the new, finer grid. However, we must once again rely upon the choice of the skeleton grid from MESA being appropriate (or once again, to rely on our controls to make it so), so that the change in variables between adjacent cells is kept within a reasonable limit such that this effect is controlled.

3.4. Other considerations. I will outline some other problems in the implementation of the Henyey code to solve the oscillation equations here, particularly focussing on how they were overcome, or worked around.

In choosing the form of the recurrence relations used in the Henyey code, multiple different expressions for analytically equivalent versions were possible. A major consideration was to ensure that inverting singular matrices (such as using $\underline{\alpha}_0^{-1}$) was avoided, which limited the possible sensible range of expressions. Even so, these different expressions were tested to discover which versions were most effective in solving the test equations, and how to express them using the fewest matrix manipulations. For the outgoing recurrence relation, there was only one essential expression, and all the others were found to be exactly analytically equivalent. For the returning recurrence relation, however, two genuinely distinct options are available. Both cases were tested and their accuracy evaluated, and case I was selected to be used. Further details can be found in appendix B.

A major obstacle to achieving the required resolution was the limitation due to the size of the available RAM. This is a result of the fact that the process to iterate from step $k + 1$ to k on the return journey requires information which was used to step from k to $k + 1$ on the outgoing journey. As such, each step is not stand-alone, and a large amount of memory was being used in defining each matrix at each location in the star for the entirety of the calculation. In order to improve this situation, I introduced some new arrays which would be used specifically to exactly what would be needed for the return journey, and only that information. Using this, each matrix array need only contain the information for the step from k to $k + 1$ at the time that that outward step is being evaluated, as the required information for the step from $k + 1$ to k on the return journey would be evaluated at that point and saved, then the matrices would be re-evaluated for the next outward step. This introduces a few arrays of dimension $2 \times 2 \times J$, but also cuts down many arrays from the previously required $2 \times 2 \times J$ to $2 \times 2 \times 2$. This solution does still hit another limit, however, as there are still some matrices which grow linearly with the resolution, so the RAM limitation is still in place, but at a suitable resolution. Also, as the resolution is controlled as a function of position in the star, the limited number of cells can be distributed such that the highest resolution is where the need is greatest, although this is not an automatic process, but must be managed manually.

4. OUTPUT

In order to ensure that the code and equations are all correct, work from a previous paper (Terquem *et al.*, 1998, figure 1) has been reproduced and the output has been compared. The previous work used a shooting method, and treated the non-adiabatic case slightly differently, but good agreement has been found between the paper's result and my own, which can be seen in figure 2. Some particular differences to note are the following: the precise form of spatial oscillations in the core varies depending on the exact parameters used in the solution (which will be explored in the following paragraphs), and the behaviour at the very surface (that is, the last $\sim 0.1\%$ of the star's radius) is significantly different, although this is due to the thin outermost radiative layer of the star, and is not thought to be a problem with the Henyey method's application in this case.

To investigate some of the limitations of this solution, some of the parameters used in the solution were varied slightly, to investigate what effect this had in the different regions of the star.

Firstly, a purely physical parameter was varied by up to 1%, the semi-major axis of the planet's orbit. This would be expected to have a slight effect on the amplitude of the response throughout the star, as a more distant planetary companion would lead to a lessened tidal effect, but it would also slightly shift the frequency of the orbit, and would therefore be expected to alter the spatial frequency of oscillations within the star. This effect can be seen in figure 3, where it is particularly notable that the amplitude of the spatial oscillations at the very centre varies hugely, from, effectively, -300 to $+500$ mm s $^{-1}$. The overall trend, however of oscillations which grow towards the centre of the core is clearly maintained, as is the decrease in spatial frequency further from the core. The transition to evanescent waves in the convective envelope (from $\frac{r}{R} \approx 0.7$) is consistent across the cases, and is very similar in amplitude (particularly given that the magnitude

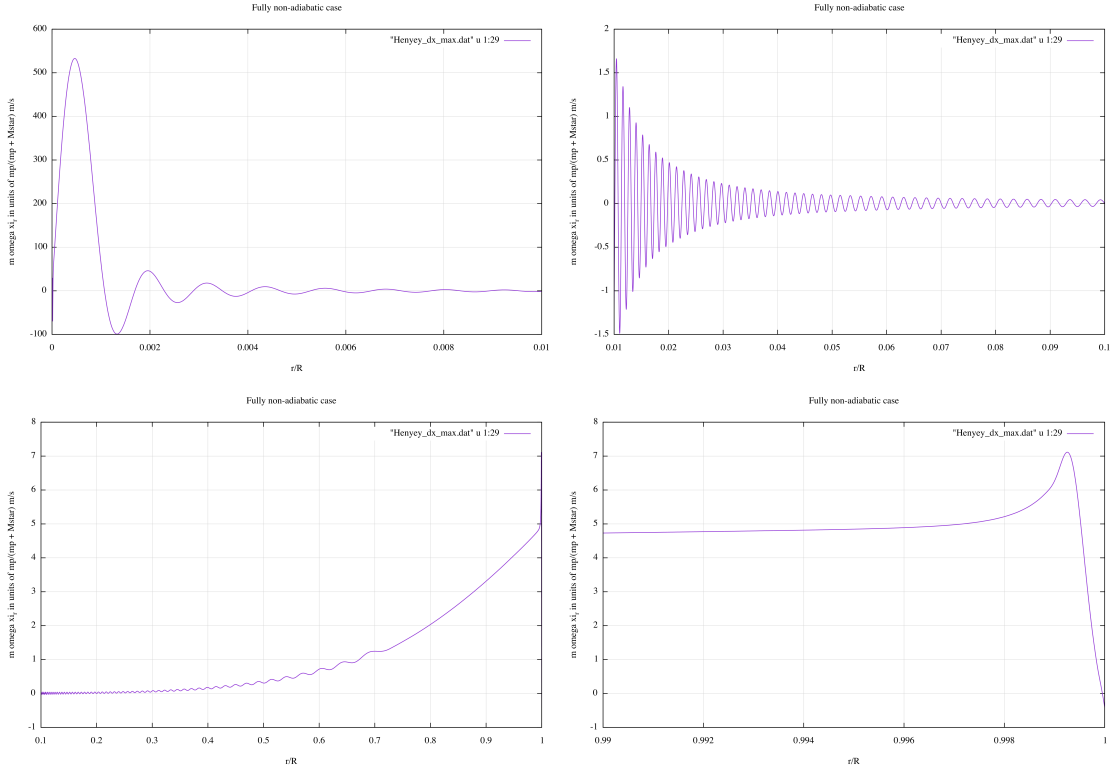


FIGURE 2. The full solution for the non-adiabatic case, showing the peak radial velocity (that is, $m\omega\xi_r$) in units of $\frac{m_p}{m_p+M_*} \text{ m s}^{-1}$, against the proportional radial distance from the centre. Four segments have been shown, as the first three reproduce the graphs in Terquem *et al.*, 1998, and the fourth highlights the behaviour in the thin radiative layer at the star's surface. As a rough guide, the y-axis is approximately in mm s^{-1}

of the tidal potential varies as D^{-3}). Overall, it seems that the observable behaviour is not particularly sensitive to small variations in D for this case, and that the patterns of behaviour in each region are unaffected, but that one should be wary of drawing precise quantitative conclusions about the oscillations in the core.

The other parameter which was varied was the resolution, the outputs of which are shown in figure 4. In this case, a flat limit was introduced across the whole star, rather than varying it to match the needed resolution in order to try to keep things as simple as possible. In all cases the resolution is sufficient to resolve the oscillations, (with the lowest resolution having at least 13 points covering the shortest spatial wavelength, and the highest resolution having at least 20 points). Similar to the case of varying D , varying the resolution has a significant effect on the amplitude of the oscillations towards the centre of the star, but has a totally negligible effect towards the surface. This may be partially due to the fact that the MESA skeleton of cells is already of a higher resolution

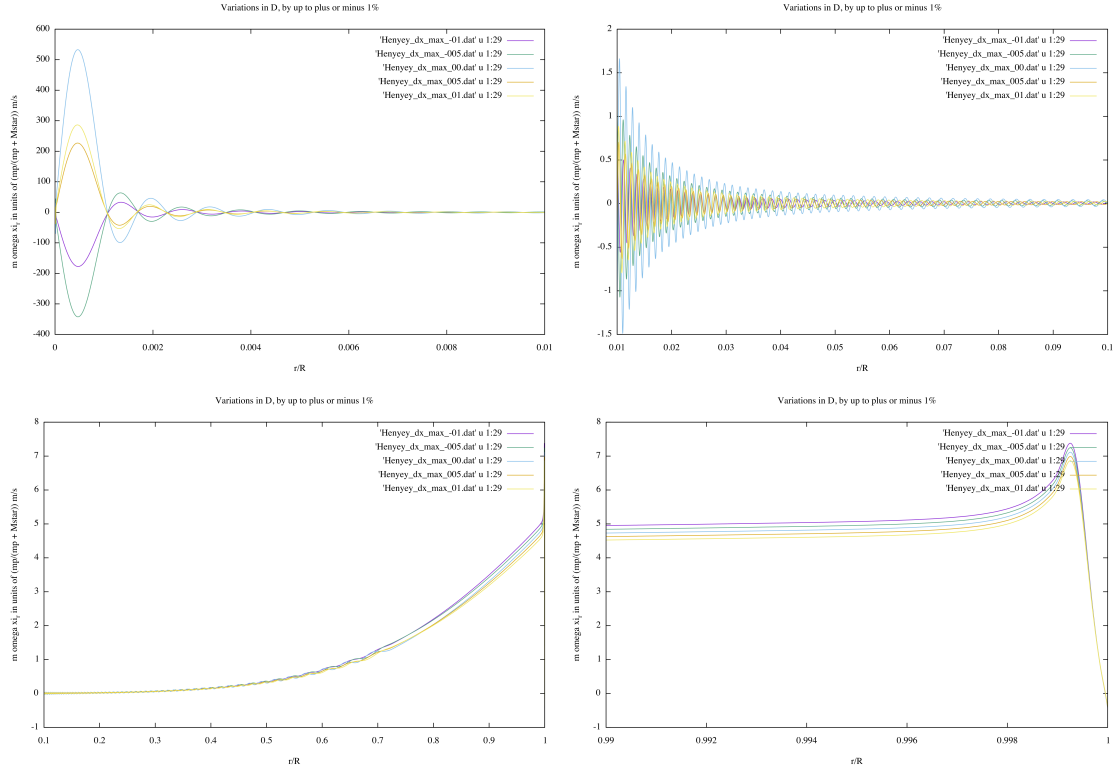


FIGURE 3. The full solution for the non-adiabatic case, showing the peak radial velocity (that is, $m\omega\xi_r$) in units of $\frac{m_p}{m_p+M_*} \text{ m s}^{-1}$, against the proportional radial distance from the centre. In these figures, the semi-major axis of the planetary companion's orbit has been varied slightly, leading to a small spread in both the amplitudes and spatial frequencies of the oscillations.

than the limits used in this case for the surface, coupled with the fact that the solution is no longer oscillatory.

Where there is variation in the amplitude, the spatial wavelengths are still unaffected, and the overall patterns of behaviour are very similar for all the resolutions. This is encouraging, as it shows that, although resolution may limit the extent to which we can extract precise quantitative data from the central regions, the nature and behaviour of the waves, both oscillatory and evanescent, seems to be unaffected. As such, whilst it is clear that a higher resolution is desirable, it does not limit the usefulness of the output any more than the physical limits in the precision of the parameters of the system do (as shown in figure 3).

A final point to consider is the validity of the assumptions made in the derivation of the equations (listed in section 1.3), to check that the solution is consistent with them. This essentially boils down to ensuring that the perturbations are small at all points throughout the star, which can be assessed by checking the output throughout the

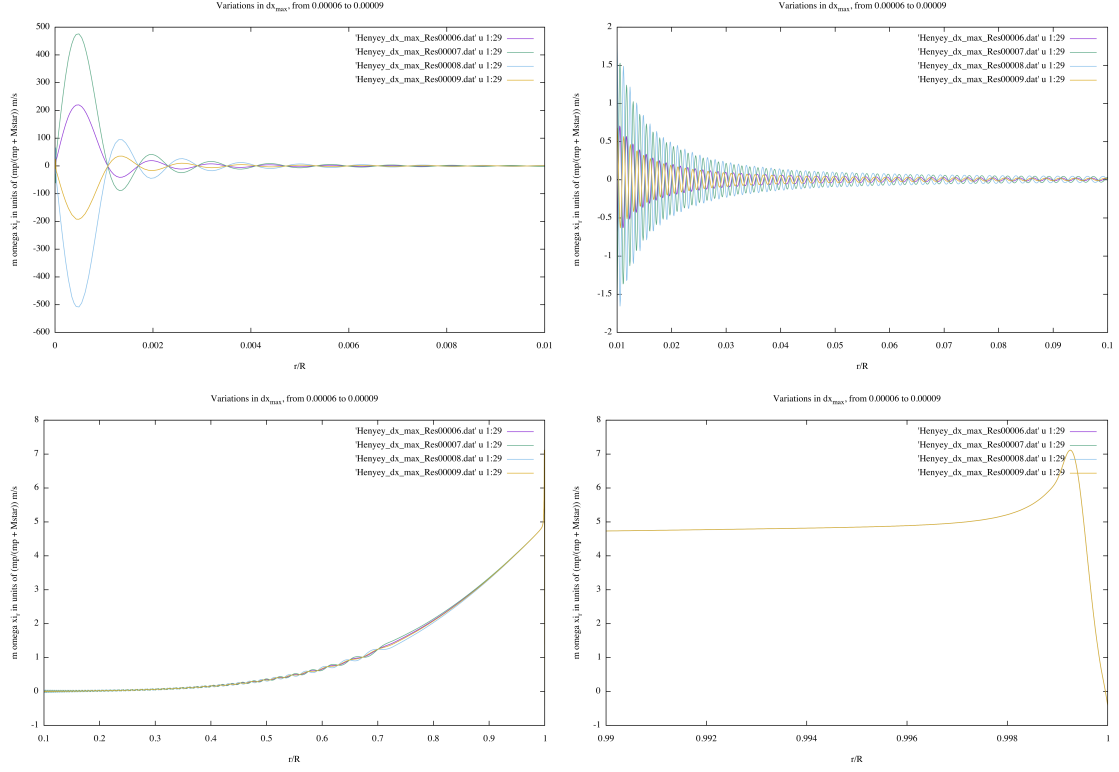


FIGURE 4. The full solution for the non-adiabatic case, showing the peak radial velocity (that is, $m\omega\xi_r$) in units of $\frac{m_p}{m_p+M_*} \text{ m s}^{-1}$, against the proportional radial distance from the centre. In these figures the maximum cell size, and therefore the resolution limit of the grid, has been varied slightly, leading to a spread in the amplitudes of the oscillations. The maximum cell size, as a proportion of the stellar radius, is plotted at 6×10^{-5} (purple line), 7×10^{-5} (green line), 8×10^{-5} (blue line), and 9×10^{-5} (orange line).

entirety of the star. Where this assumption is likely to break depends on the variables: ξ_r and F'_r are most likely to be comparable to the local equilibrium values (r and F_r) towards to core of the star; p' and T' are most likely to be comparable towards the surface. In the case tested here, other than a few points in the value of F'_r at the very core, all points are $\ll 1$. These very core points are not thought to be much of an issue, as they seem to just be an edge effect, which has no apparent impact on the rest of the solution, and quickly decays away.

Overall, the code is well tested, and reproduces previous results well. It is easy to apply to any model created in MESA, and the stability of the solution can be simply tested by investigating the effect of small variations in parameters, enabling the expected errors to be very simply and effectively assessed, and the code can be adapted and continually tested to ensure that the equations remain valid in all cases.

5. CONCLUSION

Overall, the project has started well, with the production of an effective, quick and adaptable code which can be used to accurately solve the stellar oscillation equations. The code's limitations have been explored, including both errors due to limited physical knowledge and limitations inherent in the numerical calculation.

There are many observed systems to which this code could be applied, as well as multiple different avenues of further research, which will be discussed in the section 6. The outputs of this code are useful, and will be able to be compared to observations soon, as they can be translated into both photometric and spectroscopic effects, which will enable the accuracy of stellar models to be tested, and will also lead to improved methods for detecting subsequent planets in systems with an observed Hot Jupiter.

Furthermore, the code is adaptable, in that the source of the perturbation could be changed in order to model another cause of oscillations, and that the code can be expanded to address different modes of oscillation, stellar rotation, or eccentric planetary orbits.

6. FURTHER WORK

The most immediate plan would be to extend the code to convert the solution into the photometric and spectroscopic observations which would result, and to apply this to a number of known systems with Hot Jupiters, such as Pegasi 51b, HD 189733 b and HD 209458 b. This would result in a paper, likely over the course of a few months. The assessment of different systems to find those which would have the greatest likelihood of being detected in observations would follow this.

In terms of a slightly more theoretically exploratory angle, the tidal asteroseismology of advanced stars, particularly Red Giants will be explored, to investigate the potentially observable oscillations, and how this could be used in both the testing of the structure of advanced stars, and also for the prospects of detecting multiple planets around Red Giants. This kind of investigation could also be applied to White Dwarfs, or even to stellar binaries to predict the tidal oscillations induced in both objects. Each avenue could be deepened, depending upon the success of the modelling, and the prospect for relevant observations, but this would also be likely to produce at least one paper.

The code as a whole could be broadened in its scope, by extending the realm over which the code is applicable: allowing for stellar rotation, eccentric orbits, and higher order perturbations. This would apply to all of the above in terms of extending the relevancy and scope of research, and could enable better characterisation of systems, by being able to constrain the rotation of stars by comparing the predicted and observed results. There are also published results regarding the modelled dynamical tides in stars as a result of rotation and eccentric orbits [2] against which the code could be once more tested and calibrated.

Overall, there are several possible, realistic and valuable avenues down which this research could continue, which could make predictions which could be used to potentially direct the use of observing time, and to test the accuracy of stellar modelling across a range of scenarios.

7. ACKNOWLEDGEMENTS

I would like to acknowledge the input of my supervisor, Caroline Terquem, in the form of guidance and discussion throughout this project.

I would like to acknowledge MESA, [18]. <http://mesa.sourceforge.net/index.html>

This research has made use of the NASA Exoplanet Archive, which is operated by the California Institute of Technology, under contract with the National Aeronautics and Space Administration under the Exoplanet Exploration Program.

REFERENCES

- [1] Timothy M. Brown, Ronald L. Gilliland, Robert W. Noyes, and Lawrence W. Ramsey. Detection of possible p-mode oscillations on Procyon. *The Astrophysical Journal*, 368:599, 1991.
- [2] Joshua Burkart, Eliot Quataert, Phil Arras, and Nevin N. Weinberg. Tidal asteroseismology: Kepler's KOI-54. *Monthly Notices of the Royal Astronomical Society*, 421(2):983–1006, apr 2012.
- [3] William J. Chaplin and Andrea Miglio. Asteroseismology of Solar-Type and Red-Giant Stars. 2013.
- [4] Jeffrey L. Coughlin, F. Mullally, Susan E. Thompson, Jason F. Rowe, Christopher J. Burke, David W. Latham, Natalie M. Batalha, Aviv Ofir, Billy L. Quarles, Christopher E. Henze, Angie Wolfgang, Douglas A. Caldwell, Stephen T. Bryson, Avi Shporer, Joseph Catanzarite, Rachel Ake-son, Thomas Barclay, William J. Borucki, Tabetha S. Boyajian, Jennifer R. Campbell, Jessie L. Christiansen, Forrest R. Girouard, Michael R. Haas, Steve B. Howell, Daniel Huber, Jon M. Jenkins, Jie Li, Anima Patil-Sabale, Elisa V. Quintana, Solange Ramirez, Shawn Seader, Jeffrey C. Smith, Peter Tenenbaum, Joseph D. Twicken, and Khadeejah A. Zamudio. PLANETARY CANDIDATES OBSERVED BY <i>KEPLER</i>. VII. THE FIRST FULLY UNIFORM CATALOG BASED ON THE ENTIRE 48-MONTH DATA SET (Q1Q17 DR24). *The Astrophysical Journal Supplement Series*, 224(1):12, 2016.
- [5] N Crouzet, X Bonfils, X Delfosse, I Boisse, G Hébrard, T Forveille, J. F. Donati, F Bouchy, C Moutou, R Doyon, E. Artigau, L. Albert, L. Malo, A. Lecavelier des Etangs, and A. Santerne. Follow-up and characterization of the TESS exoplanets with SOPHIE, SPIRou, and JWST. page 5, 2017.
- [6] M. S. Cunha, C. Aerts, J. Christensen-Dalsgaard, A. Baglin, L. Bigot, T. M. Brown, C. Catala, O. L. Creevey, A. Domiciano De Souza, P. Eggenberger, P. J.V. Garcia, F. Grundahl, P. Kervella, D. W. Kurtz, P. Mathias, A. Miglio, M. J.P.F.G. Monteiro, G. Perrin, F. P. Pijpers, D. Pourbaix, A. Quirrenbach, K. Rousselet-Perraut, T. C. Teixeira, F. Thévenin, and M. J. Thompson. Asteroseismology and interferometry. *Astronomy and Astrophysics Review*, 14(3-4):217–360, 2007.
- [7] Maria Pia Di Mauro. A review on Asteroseismology. pages 0–29, 2017.
- [8] A Garg, K H Cook, S Nikolaev, M E Huber, A Rest, A C Becker, P Challis, A Clocchiatti, G Miknaitis, D Minniti, L Morelli, K Olsen, J L Prieto, N B Suntzeff, and D L Welch. HIGH-AMPLITUDE δ -SCUTIS IN THE LARGE MAGELLANIC CLOUD. pages 328–338, 2010.
- [9] A. B. Hart. Motions in the Sun at the Photospheric Level IV. The Equatorial Rotation and Possible Velocity Fields in the Photosphere. *Monthly Notices of the Royal Astronomical Society*, 114(1):17–38, feb 1954.
- [10] L G Henyey, J E Forbes, and N L Gould. A New Method of Automatic Computation of Stellar Evolution. *Astrophysical Journal*, 139:306, 1964.
- [11] Dorrit Hoffleit. History of the Discovery of Mira Stars. *JAAVSO*, 25:115 – 136, 1997.
- [12] Lauri Jetsu and Sebastian Porceddu. Shifting Milestones of Natural Sciences: The Ancient Egyptian Discovery of Algol's Period Confirmed. *PLoS ONE*, 10(12), 2015.
- [13] H Kjeldsen, T R Bedding, I K Baldry, H Bruntt, R P Butler, D A Fischer, S Frandsen, E L Gates, F Grundahl, K Lang, G W Marcy, A Misch, and S S Vogt. Confirmation of Solar-like Oscillations in η Bootis. *The Astronomical Journal*, 126:1483, 2003.
- [14] D W Latham, R P Stefanik, T Mazeh, M Mayor, and G Burki. The unseen companion of HD114762 - A probable brown dwarf, 1989.

- [15] Barry F. Madore and Wendy L. Freedman. The Cepheid distance scale. *Publications of the Astronomical Society of the Pacific*, 103(September 2013):933, 1991.
- [16] M Mayor and D Queloz. A Jupiter-mass companion to a solar type star. *Nature*, 378(1993):355–359, 1995.
- [17] NASA Exoplanet Science Institute. NASA Exoplanet Archive.
- [18] Bill Paxton, Lars Bildsten, Aaron Dotter, Falk Herwig, Pierre Lesaffre, and Frank Timmes. MODULES FOR EXPERIMENTS IN STELLAR ASTROPHYSICS (MESA). *The Astrophysical Journal Supplement Series*, 192:3–35, 2011.
- [19] Bill Paxton, Pablo Marchant, Josiah Schwab, Evan B Bauer, Lars Bildsten, Matteo Cantiello, Luc Dessart, R Farmer, H Hu, N Langer, R H D Townsend, Dean M Townsley, and F X Timmes. MODULES FOR EXPERIMENTS IN STELLAR ASTROPHYSICS (MESA): BINARIES, PULSATIONS, AND EXPLOSIONS. *The Astrophysical Journal Supplement Series*, 220(1):15, sep 2015.
- [20] H.~H. Plaskett. A Variation in the Solar Rotation. *\Apj*, 43:145, 1916.
- [21] Roger K. Ulrich. The Five-Minute Oscillations on the Solar Surface. *The Astrophysical Journal*, 162:993, dec 1970.
- [22] Sharon Xuesong Wang, Jason T. Wright, William Cochran, Stephen R. Kane, Gregory W. Henry, Matthew J. Payne, Michael Endl, Phillip J. MacQueen, Jeff A. Valenti, Victoria Antoci, Diana Dragomir, Jaymie M. Matthews, Andrew W. Howard, Geoffrey W. Marcy, Howard Isaacson, Eric B. Ford, Suvrath Mahadevan, and Kaspar von Braun. THE DISCOVERY OF HD 37605 <i>c</i> AND A DISPOSITIVE NULL DETECTION OF TRANSITS OF HD 37605 <i>b</i>. *The Astrophysical Journal*, 761(1):46, 2012.
- [23] Joshua N. Winn and Daniel C. Fabrycky. The Occurrence and Architecture of Exoplanetary Systems. pages 1–41, 2014.

APPENDIX A. STELLAR OSCILLATION EQUATIONS

APPENDIX B. DETAILED EXPLANATION OF THE GENERAL HENYET METHOD